Mathematical Modelling on Dynamics of Multi-variant SARS-CoV-2 Virus: Estimating Delta and Omicron Variant Impact on COVID-19

Sadhana Gupta, Rupali*, Yogendra Kumar Rajoria, and Govind Prasad Sahu

***Abstract*—COVID-19, caused by the novel coronavirus SARS-CoV-2, resulted in health threats on a global scale. We developed a modified SIQR mathematical model to study the transmission dynamics of the SARS-CoV-2 with two different variants: Delta and Omicron. First, we establish the well-posedness of our model and then analyse the local and global stability of the model at the equilibrium points. Further, we compute the reproduction number denoted by R_0 analytically and numerically. The model analysis shows that the disease-free equilibrium point remains globally asymptotically stable as long as the value of R_0 is below one. While if R_0 exceeds one, the stability of disease-free equilibrium becomes unstable. A numerical simulation of the mathematical model was carried out to understand its quantitative behaviour. The sensitivity analysis is performed to identify the parameters which are sensitive to reproduction number, R_0. The results of the sensitivity analysis show that the transmission rate and the birth rate were the most sensitive parameters for R_0. A PRCC-sensitive analysis is also performed to quantify uncertainty and sensitivity at the level of the infected class. Further, we try to explore the measures to curb the incidence of COVID-19 due to delta and omicron variants.**

***Index Terms*—SIQR model, COVID-19, Delta and Omicron, Local and global stability, Reproduction number, Multi-variants, Sensitivity.**

I. Introduction

COVID-19, which was first identified in 2019 in Wuhan, China, spread quickly to several nations and regions of the world due to its high contagiousness, causing disruption [1]–[4]. The virus from the SARS-CoV family was named SARS-CoV-2, and the disease was named COVID-19 by WHO in February 2020. On 30th Jan 2020, WHO announced it as a worldwide public health emergency. The mortality due to COVID-19 was very high globally. Among the different strains of the SARS-CoV-2 virus, the Delta variant was highly contagious, causing the highest mortality. It is crucial to have a better knowledge of the characteristics linked with the virus in order to prevent future pandemics. It has been demonstrated that mathematical models are useful tools to study the dynamics of diseases and generate evidence for decision-making in global health [5]. In order to investigate the COVID-19 spread pattern, various mathematical and numerical models have been developed using ordinary differential equations and delay differential equations. A SIR model is developed [4] to investigate the effects of the pandemic caused by the transmission of the rare COVID-19 disease. Ming et al. [6] studied an optimized SIR-type model and forecasted the COVID-19 infected cases and the burden on isolation wards and ICUs. In order to comprehend COVID-19 illness, certain compartment models were created, some of which may be found in [7]–[17]. Using an optimum control method, the impact of enhanced control and mitigation measures such as isolation, screening, medical treatment, and quarantine was investigated by [18]–[24]. To determine the critical inflammatory factors and the role of a combination of medical treatment of COVID-19, a simple within-host tool model was created in [7]–[12]. Compartmental models were proposed to predict the COVID-19 spread in India in [25]. Analysis of local and global stability was performed with reference to (R_0) for the model equilibria. The study reveals that the transmission rate was very effective in lowering R_0. The authors traced the COVID-19 outbreak throughout Indian states using the SMAART RAPID Tracker in [26]. The study emphasized the necessity of a nation-centric strategy for tracking and controlling the COVID-19 pandemic. The factors that probably led to the third wave in India were examined by the authors using a compartmental model in [27]. To prepare for future waves of COVID-19, this study suggests increasing vaccination coverage. Similarly, [28] addressed the importance of using NPIs effectively to lower the death rate in India. A study by Sukandar et al. [29] analyzed a Susceptible-Exposed-Infectious-Recovered (SEIR) based mathematical model to effectively measure the transmission indicators per day to control the spread of the epidemic. Zhang et al. [30] introduced a modified SEIR model to enhance decision-making during COVID-19 outbreaks, providing more accurate infection trend predictions. This model supported effective resource allocation and policy formulation during pandemics. Viruses evolve into different variants as they get multiple hosts to mutate. The SARS-CoV-2 virus also evolved into many variants, to name a few variants of concern: Alpha, Delta, and Omicron. The Delta variant of COVID-19 caused severe complications in the infected and soon overwhelmed the health system in many countries, including India, with increased demands for hospitalization, oxygen, ICU, and ventilators.

On the other hand, the Omicron variant had higher transmissibility and spread fast. Thus, Compared to the Delta version, there were more infected people, but because the

Manuscript received March 14, 2024; revised November 27, 2024.

Sadhana Gupta is a Ph.D scholar of the School of Basic and Applied Sciences, K.R. Mangalam University, Gurugram, Haryana 122103 India. (e-mail: sadhanag85@gmail.com,paramsadhana13@gmail.com).

Rupali is an assistant professor in School of Basic and Applied Sciences, K.R. Mangalam University, Gurugram, Haryana 122103 India. (e-mail: rupali@krmangalam.edu.in).

Yogendra Kumar Rajoria is an associate professor in the School of Basic and Applied Sciences, K.R. Mangalam University, Gurugram, Haryana 122103, India. (e-mail: yogendrakr.rajoria@krmangalam.edu.in).

Govind Prasad Sahu is an Assistant Professor of Mathematics at Center for Basic Sciences, Pt. Ravishankar Shukla University, Raipur, Chhattisgarh 492010 India (e-mail: govind3012@gmail.com).

Omicron variant's infections were not as severe, there were fewer hospitalizations and fewer case deaths. González-Parra et al. [31] constructed a mathematical model for the analysis of the Omicron strain of COVID-19 and concluded that although the Omicron strain has a low fatality rate, it can still cause a number of deaths. COVID-19 vaccinations are successful in preventing serious diseases. The two omicron sub-lineages (offshoots) that are most critical are BA.5 and BA.2.12.1. According to the CDC [32], infections caused due to BA.5 are around 88% in the United States and were genetically sequenced in August 2022. In order to comprehend the variants of SARS-CoV-2 can be found in [33]–[35]. To better understand the variants of the SARS-CoV-2 virus in the present study, we develop a four-compartment model considering the transmission of infection through Delta and Omicron variants. The manuscript work is structured as follows: Section II presents a mathematical model based on SIQR for the study of the omicron and delta variants presenting detailed factors and variables, whereas, in Section III, we have discussed the effectiveness and positive response of the solutions. Section IV describes the stability analysis of various equilibrium points admitted by the SIQR model. Section V presents the numerical simulation and sensitivity analysis of factors, while Section VI presents the discussion and conclusion part.

II. Formulation of Mathematical SIQR) Model

This paper uses four dimensions to investigate a mathematical SIQR model for novel COVID-19: susceptible: S, infected: I, quarantine: Q, and recovered: R. Differential equations are used to formulate the model. The population is thought to be evenly distributed, and diseases are spread through direct contact among susceptible and infected people and by the mobility of people from the susceptible and infected classes. Let N be the entire population of the region under study at any given time t, which is the sum of four sub-populations. Let k be the rate of individual contact tracing, with a fraction $1-k$ responsible for spreading infection and the remainder quarantined. The population's natural death rate in each compartment is represented by μ. The virus transmission rates for the delta and omicron variants are represented by β_D and β_o, respectively. The infective and quarantine populations' recovery rates are γ while the mortality rates of delta and omicron variants are α_D and α_o, respectively. The rate at which infected people are quarantined is expected to be σ. The schematics flow diagram is represented in Fig. 1 to comprehend COVID-19 interactions. The model's dynamic is represented as follows in the form of a differential equation:

$$\frac{dS}{dt} = A-(\beta_o+\beta_D)SI-\mu S \quad (1)$$

$$\frac{dI}{dt} = (1-k)(\beta_o+\beta_D)SI - (\alpha_o+\alpha_D+\mu+\sigma+\gamma)I \quad (2)$$

$$\frac{dQ}{dt} = k(\beta_o+\beta_D)SI+\sigma I-(\mu+\gamma)Q \quad (3)$$

$$\frac{dR}{dt} = \gamma(I+Q)-\mu R. \quad (4)$$

Along with initial conditions $S(0)>0, I(0)\geq 0, Q(0)\geq 0, R(0)\geq 0$ at $t=0$ in which $\alpha_D>\alpha_o$ and $\beta_D<\beta_o$. The following Table I provides the definitions of each model component and parameter.

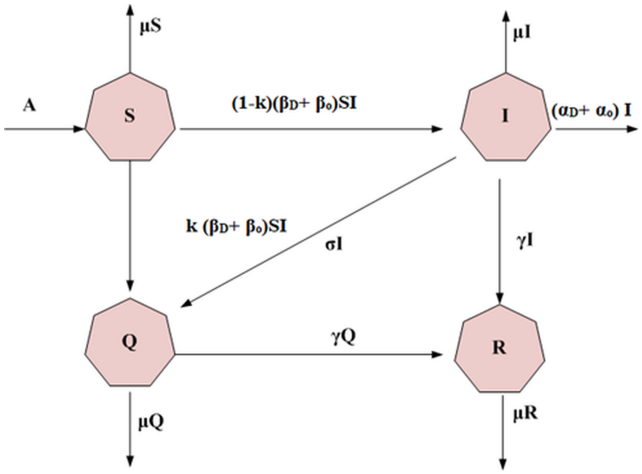

Fig. 1: Schematic flow diagram of the SIQR COVID-19 model

TABLE I: Variables and Parameters used in the Differential Formulation

Parameter	Description	Parameter	Description
S	Size of susceptible population	σ	Isolation rate of infectives
I	Size of infected population	β_o	Transmission rate of omicron variant
Q	Size of quarantined population	k	Rate of contact tracing
R	Size of recovered population	α_D	Death rate due to delta variant
A	Recruitment rate	α_o	Death rate due to omicron variant
β_D	Transmission rate of delta variant	γ	Recovery rate
μ	Natural death rate		

III. Positivity and Bounded Conditions

In this section, we demonstrate that the solutions of the system of equations, as defined in Eqs. (1)-(4), remain positive and bounded for all time.

A. Positivity

Theorem 1. *The solutions of the system given in Eqs. (1)-(4) with conditions, $S(0)>0, I(0)\geq 0, Q(0)\geq 0, R(0)\geq 0$ are all positive, for all non-negative t (i.e. $t\geq 0$).*

Proof: From the system of equations given in Eqs. (1) -(4) the following expression is obtained

$$\frac{dI}{dt} \geq -(\alpha_D+\alpha_o+\mu+\sigma+\gamma)I$$

$$\text{or } \frac{dI}{I} \geq -(\alpha_D+\alpha_o+\mu+\sigma+\gamma)dt.$$

Taking integration, we obtain

$$I(t) \geq e^{-(a_D+a_o+\mu+\sigma+\gamma)t}.$$

Letting limit as $t\to\infty$ in the above expression, we get $\lim I(t)\geq 0$. From Eqs. (3) we have

$$\frac{dQ}{dt} \geq -(\mu-\gamma)Q$$

$$\text{or } \frac{dQ}{Q} \geq -(\mu-\gamma)dt.$$

Upon integrating the above equations, the following expression is obtained

$$Q(t) \geq \exp^{-(\mu-\gamma)t}.$$

Again taking limit as $t \to \infty$

$$\lim Q(t) \geq 0.$$

Similarly, it is seen that limit $t \to \infty$ yields $\lim R(t) \geq 0$ and $\lim S(t) \geq 0$.

Thus, we find that all the population, i.e., Susceptible: S, Infected: I, Quarantined: Q and Recovered: R at any time t, are non-negative. ■

B. Boundedness

Let's write $N(t) = S(t) + I(t) + Q(t) + R(t)$ to represent the total population at any time t. Taking derivative of $N(t)$ with respect to t, following expression is obtained:

$$\begin{aligned}\frac{dN}{dt} &= \frac{dS}{dt} + \frac{dI}{dt} + \frac{dQ}{dt} + \frac{dR}{dt} \\ &= A - \mu N - (\alpha_D + \alpha_o) I \\ &\leq A - \mu N.\end{aligned}$$

At this point integrating factor is obtained as $e^{\mu t}$. Consequently after integration we have, $N(t) \leq \frac{A}{\mu} + ce^{-\mu t}$, then as $t \to \infty$, we get $N(t) \leq \frac{A}{\mu}$.

As a result, we have demonstrated that the combination in Eqs. (1) -(4) is constructive and limited now. The following set provides the physiologically variable region.

$$\Omega = \{(S(t); I(t); Q(t); R(t)) \in \mathbb{R}^4_+; S(t) + I(t) + Q(t) + R(t) \leq \frac{A}{\mu}\}.$$

IV. STABILITY AND ANALYSIS FOR EQUILIBRIUM POINTS

The structure defined by Eqs. (1) -(4) permits two equilibria, specifically, the disease-free equilibrium E_0 and equilibrium with infection E_1. Here $E_0 = \left(\frac{A}{\mu}, 0, 0, 0\right)$ and endemic equilibrium $E_1 = (S^*, I^*, Q^*, R^*)$, where

$$S^* = \frac{A}{(\beta_D + \beta_o) I^* + \mu},$$

$$Q^* = \frac{kA(\beta_D + \beta_o) I^*}{((\beta_D + \beta_o) I^* + \mu)(\mu + \gamma)} + \frac{\sigma I^*}{\mu + \gamma},$$

$$R^* = \frac{\gamma(I^* + Q^*)}{\mu},$$

$$I^* = \frac{A(1-k)(\beta_D + \beta_o) - \mu(\mu_D + \mu_o + \sigma + \gamma + \mu)}{(\beta_D + \beta_o)(\mu_D + \mu_o + \sigma + \gamma + \mu)}.$$

A. Basic Reproduction Number

The basic reproduction number, defined as the average number of secondary cases produced per original/ primary case in an infection-free population, is calculated using the approach of next-generation matrices as in [36]. There are two states (I, Q) having infection in the system defined by Eqs. (1) -(4). To get the basic reproduction number, we construct the Jacobian matrix of the infected states at the infection-free equilibrium. We have determined the Jacobian matrix at infection-free equilibrium E_0 as follows:

$$\mathrm{J}(\mathrm{E}_0) = \begin{bmatrix} \frac{A(1-k)(\beta_D+\beta_o)}{\mu} - (\alpha_D + \alpha_o + \mu + \gamma + \sigma) & 0 \\ \frac{kA(\beta_D+\beta_o)}{\mu} + \sigma & -(\mu+\gamma) \end{bmatrix}$$ The above Jacobian matrix can be rewritten as $J(E_0) = (F + V)$ where F matrix represents the spread of a new infection and V matrix represents state changes, such as removal due to death or recovery.

The components of the F matrix and V matrix are defined as

$$F = \begin{bmatrix} \frac{A(1-k)(\beta_D+\beta_o)}{\mu} & 0 \\ \frac{kA(\beta_D+\beta_o)}{\mu} & 0 \end{bmatrix} \text{ and}$$

$$V = \begin{bmatrix} -(\alpha_D + \alpha_o + \mu + \gamma + \sigma) & 0 \\ \sigma & -(\mu+\gamma) \end{bmatrix}, \text{so}$$

$$FV^{-1} = \begin{bmatrix} \frac{A(1-k)(\beta_D+\beta_o)}{\mu(\alpha_D+\alpha_o+\mu+\gamma+\sigma)} & 0 \\ 0 & 0 \end{bmatrix}.$$

The dominant eigenvalue of the matrix FV^{-1}, denoted by the parameter λ, is given as

$$\lambda = \frac{A(1-k)(\beta_D + \beta_o)}{\mu(\alpha_D + \alpha_o + \mu + \gamma + \sigma)}.$$

As a result, the value of R_0 (basic reproduction number), which is equal to the dominant eigenvalue of the matrix FV^{-1} is given as follows:

$$\mathrm{R}_0 = \frac{A(1-k)(\beta_D + \beta_o)}{\mu(\alpha_D + \alpha_o + \mu + \gamma + \sigma)}. \tag{5}$$

B. LOCAL AND GLOBAL DYNAMICS STABILITY ANALYSIS FOR E_0

Jacobian matrix at the infection-free equilibrium E_0 for the system equations (1) -(4) is given as:

$$J(E_0) = \begin{pmatrix} -\mu & \frac{A(\beta_D+\beta_o)}{\mu} & 0 & 0 \\ 0 & \frac{A(1-k)(\beta_D+\beta_o)}{\mu} & 0 & 0 \\ 0 & \frac{Ak(\beta_D+\beta_o)}{\mu} + \sigma & -(\mu+\gamma) & 0 \\ 0 & \gamma & \gamma & -\mu \end{pmatrix}.$$

The characteristics equation for the Jacobian Matrix $J(E_0)$ is given by

$$\lambda^4 + P\lambda^3 + Q\lambda^2 + R\lambda + T = 0, \tag{6}$$

where $a = \mu, b = \mu + \gamma$, $c = \alpha_D + \alpha_o + \mu + \gamma + \sigma$ and

$P = ab + b + c(1 - R_0)$,

$\mathrm{Q} = a^2 + bc(1 - R_0) + ab^2 + abc(1 - R_0)$,

$R = a^2 b(1 + c(1 - R_0)) + ac(1 - R_0)\left(a + b^2\right)$,

$T = a^2 bc(1 - R_0)$.

We can clearly see that P, Q, R, T are all positive (i.e. $P > 0, Q > 0, R > 0, T > 0$) if $R_0 < 1$ and also $PQR - R^2 - P^2 T > 0$ for $R_0 < 1$. Thus, by using Hurwitz's theorem, we find that if R_0 is less than one, the infection-free equilibrium point E_0 is locally asymptotically stable while it is unstable for $R_0 > 1$.

C. GLOBAL STABILITY FOR E_0

Here, we apply the approach described by Castillo-Chavez et al. [37]. To determine the global stability of the infection-free equilibrium E_0. Take into account the system defined below, $\frac{dX}{dt} = F(X, Y)$, where X stands for the compartments of the population that are uninfected and Y for those that are,

including latent, infectious, etc. In this case, $G(X,0)=0$ is satisfied by the function G. The equilibrium point of the aforementioned general system of equations is denoted by $U_0=\left(X_0,\overline{0}\right)$. If the given below conditions are satisfied, then U_0 for the aforementioned general system of equations is globally asymptotically stable if the following two criteria are fulfilled, assuming $R_0<1$.

If the given below conditions are satisfied then U_0 is globally asymptotically stable with the above-mentioned general system provided $R_0<1$.

A_1 : Global asymptotically stable X_0 exists for the subsystem $\frac{dx}{dt}=F(X,0)$.

A_2: The function $G=G(X,Y)$ can be represented as $G(X,Y)=AY-\hat{G}(X,Y)$, where $\hat{G}_r(X,Y)\geq 0\forall(X,Y)$, in the feasible region Ω for j = 1,2,3 and $A=D_YG(X,Y)$ when $X=X_0$ and $Y=\overline{0}$ is an M-matrix (matrix with positive off-diagonal elements).

Note that the system is defined in Eqs. (1) -(4) can be expressed in the aforementioned general system format, and both two cases, A_1 and A_2, are satisfied. We shall demonstrate the global stability of disease-free equilibrium $E_0=\left(\frac{A}{\mu},0,0,0\right)$.

On comparing the aforementioned general system, i.e. $\frac{dX}{dt}=F(X,Y)$ with the system given in Eqs. (1) -(4), Where F and G are presented as follows:

$$F(X,Y)=A-A_1SI-\mu S$$

$$G(X,Y)=\begin{pmatrix}(1-k)A_1SI-A_2I, & kA_1SI+\sigma I\\ -(\mu+\gamma)Q, & \gamma(I+Q)-\mu R\end{pmatrix}$$

Where $X=S,Y=(I,Q,R),A_1=\beta_D+\beta_o$, and $A_2=(\alpha_D+\alpha_o+\mu+\sigma+\gamma)$.

The infection-free equilibrium point is denoted by $U_0=\left(X_0,\overline{0}\right)$, in which the arguments are given as $X_0=\frac{A}{\mu}$ and $\overline{0}=(0,0,0)$ We may infer that U_0 is locally asymptotically stable iff $R_0<1$ from the stability analysis of E_0. It is obvious that $G(X,\overline{0})=(0,\overline{0})$. We now demonstrate that $X_0=\left(\frac{A}{\mu}\right)$ is globally asymptotically stable for the subsystem

$$\frac{\mathrm{d}S}{dt}=F(S,\overline{0})=A-\mu S \tag{7}$$

Here, it is obtained that the integrating factor is $e^{\mu t}$ and therefore after performing integrating, the above equation (7) leads to the following relation, $S(t)e^{\mu t}=\frac{Ae^{\mu t}}{\mu}+c$.

Letting limit $t\to\infty$, we obtain $S(t)=\frac{A}{\mu}$, which does not depend on c. Because of this independence, it follows that $X_0=\frac{A}{\mu}$ is globally asymptotically stable for the subsystem $\frac{dS}{dt}=A-\mu S$. As a result, assumption A_1 holds.

We shall now demonstrate that assumption A_2 is true. We will start by locating the matrix A. Theoretically, when $(X,Y)=\left(X_0,\overline{0}\right),A=D_YG(X,Y)$, where

$$D_YG(X,Y)=\begin{bmatrix}(1-k)A_1S-A_2 & 0 & 0\\ KA_1S+\sigma & -(\mu+\gamma) & 0\\ \gamma & \gamma & -\mu\end{bmatrix}.$$

At the points $(X,Y)=\left(X_0,\overline{0}\right)$, leads to the following

$$A=\begin{bmatrix}(1-k)A_1\frac{A}{\mu}-A_2 & 0 & 0\\ KA_1\frac{A}{\mu}+\sigma & -(\mu+\gamma) & 0\\ \gamma & \gamma & -\mu\end{bmatrix}.$$

Matrix A clearly has positive off-diagonal elements. As a consequence, A represents an M-matrix. Using $\hat{G}(X,Y)=AY-G(X,Y)$, we obtain,

$$\hat{G}(X,Y)=\begin{bmatrix}\widehat{G_1}(X,Y)\\ \widehat{G_2}(X,Y)\\ \widehat{G_3}(X,Y)\end{bmatrix}=\begin{bmatrix}(1-k)A_1I\left(\frac{A}{\mu}-S\right)\\ KA_1I\left(\frac{A}{\mu}-S\right)\\ 0\end{bmatrix}.$$

Since $S(t)+I(t)+Q(t)+R(t)\leq\frac{A}{\mu}$ we find that $S(t)\leq\frac{A}{\mu}$. Hence $\widehat{G_1}\geq 0,\widehat{G_z}\geq 0$ and $\widehat{G_3}(X,Y)=0$. Hence, if the assumptions A_1 and A_2 are fulfilled, then E_0 is globally asymptotically stable under $R_0<1$.

D. STABILITY ANALYSIS OF E_1

The Jacobian matrix at the infected equilibrium E_1 for the system described in Eqs. (1) -(4) is obtained by $\mathbf{J}_{E_1}=$

$$\begin{bmatrix}-(\beta_D+\beta_o)I^*-\mu & -(\beta_D+\beta_o)\\ (1-k)(\beta_D+\beta_o)I^* & (1-k)(\beta_D+\beta_o)S^*-(\alpha_D\\ k(\beta_D+\beta_o)I^* & k(\beta_D+\beta_o)S^*\\ 0 & \gamma\end{bmatrix}.$$

Evaluating the eigenvalues for $J(E_1)$ we find that the two eigenvalues are $\lambda_1=-\mu$ and $\lambda_2=-(\mu+\gamma)$. Other eigenvalues are the two roots of the quadratic equation given by

$$\lambda^2-(M_{11}+M_{22})\lambda+(M_{11}M_{22}-M_{12}M_{21})=0, \tag{8}$$

where

$M_{11}=-(\beta_D+\beta_o)I^*-\mu, M_{12}=-(\beta_D+\beta_o)S^*,$

$M_{22}=(1-k)(\beta_D+\beta_o)S^*-(\alpha_D+\alpha_o+\gamma+\sigma+\mu),$

$M_{21}=(1-k)(\beta_D+\beta_o)I^*.$

From the equation defined in Eqs.(8) we find that both the roots are negative provided $(M_{11}+M_{22})<0$ and $(M_{11}M_{22}-M_{12}M_{21})>0$. We see that all the eigenvalues for the matrix $J(E_1)$ are negative given that $(M_{11}+\ M_{22})<0$ and $(M_{11}M_{22}-M_{12}M_{21})>0$. Thus we observe that the infected equilibrium point E_1 exists and are asymptotically stable under the conditions $(M_{11}+M_{22})<0$ and $(M_{11}M_{22}-M_{1221})>0$.

V. NUMERICAL SIMULATION

Numerical simulations are carried out in this section to demonstrate and validate the findings of the Local and Global Dynamics section. MATLAB software is used to validate the theoretical conclusions for a set of model parameters. Table II summarises all of the parameter values utilized for the simulation. From the theoretical analysis, we know that the

TABLE II: LIST OF PARAMETER VALUES-I

Symbols	Values	Source
A	10.48	[38]
k	0.2	assumed
μ	0.00714	[38]
β_D	0.25172	[38]
β_o	0.01752	Assumed
α_D	0.0484	Assumed
α_o	0.048	[38]
γ	0.0123	[38]

infected equilibrium E_1 is also locally asymptotically stable whenever $(M_{11}+M_{22})<0$ and $(M_{11}M_{22}-M_{12}M_{21})>0$. With the parameter values from Table II, the above two

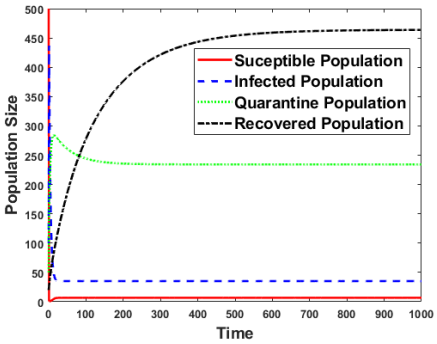

Fig. 2: The local asymptotic stability of E_1 of the system (1) -(4)

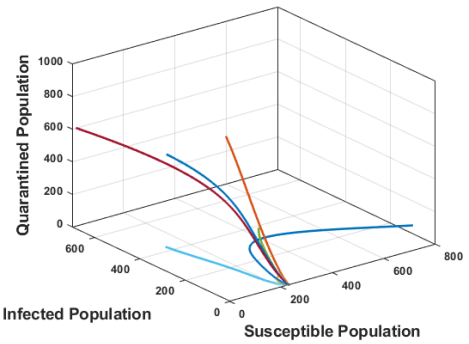

Fig. 4: The global stability of E_0 for the system of equations Eqs.(1) -(4)

conditions were found to be satisfied, and the value of E_1 was calculated to be $(7.62, 31.13, 266.21, 515.82)$. With the parameter values from Table II, we simulate the system of equations given in Eqs. (1) -(4) with the initial values $(500, 400, 50, 50)$. From Fig. 2, we see that the solution starts with $(500, 400, 50, 50)$ and reaches the infected equilibrium $E_1 = (7.62, 31.13, 266.21, 515.82)$ and remains constant. This demonstrates the locally asymptotically stable of E_1.

Considering $\mu = 0.45, k = 0.1$, and the other parameter values from Table II, we find that $R_0 < 1$. The disease-free equilibrium point E_0 was calculated to be $(23, 0, 0, 0)$. Since $R_0 < 1$, from the result proved in the previous section, the infection-free equilibrium point, $E_0 = (23, 3, 0, 0)$ is globally asymptotically stable for the system (1) - (4). In Fig. 3, taking initial condition $(500, 100, 50, 30)$ the system of equations given in Eqs. (1) - (4) were simulated and it was found that the solution of the system in Eqs. (1) - (4) reaches E_0 and remains constant. In Figure 4, we took various initial conditions and simulated the system and we found that if the model parameter values are chosen such that $R_0 < 1$, the solution always converges to the infection-free equilibrium E_0. Figure 4 describes the system's global stability at the infection-free equilibrium E_0 of the system in Eqs. (1) - (4).

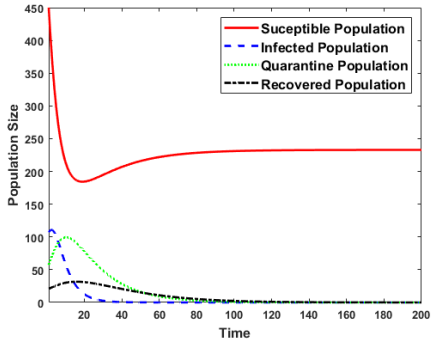

Fig. 3: The global stability of E_0 for the system of equations Eqs.(1) -(4)

A. Sensitivity and Elasticity

The basic reproduction number represented by R_0 plays a crucial role in any model. We have found the expression for R_0, which is given by, $\mathrm{R}_0 = \frac{A(1-k)(\beta_D+\beta_o)}{\mu(\alpha_D+\alpha_o+\mu+\gamma+\sigma)}$. In order to determine the best control measures, it's critical to understand the many transmission-related aspects and factors. The sensitivity index of R_0 with respect to a parameter μ is $\frac{\partial R_0}{\partial \mu}$. An additional measure is the elasticity index (Normalized Sensitivity Index), which is represented by the symbol $\phi_\mu^{R_0}$, measure the relative change of R_0 with respect to μ and is defined as $\phi_\mu^{R_0} = \frac{\partial R_0}{\partial \mu} . \frac{\mu}{R_0}$ The value of the parameter determines its relative relevance, while the elasticity index's sign shows whether the value of R_0 increases (+ sign) or decreases (- sign), with respect to the values of parameters [39]–[41].

The elasticity indices of each of the parameters of R_0 are calculated by taking parameter values described in Table II and are presented in the following Table III. The elastic index of parameters A, β_D, β_o, are positive and the remaining is negative. This implies that the increase in the values of these parameters increases R_0, whereas an increase in the values of parameters μ, γ, and α_D, α_o, and σ decreases R_0. For parameter A, we see that $\phi_\beta^{R_0} = 1$. With this, it is concluded that an increase (decrease) of β by $x\%$ increases (decreases) R_0 by $x\%$.

The elasticity indices of R_0 with the model parameters are given as follows:

$$\phi_A^{R_0} = \frac{\partial R_0}{\partial A}\frac{A}{R_0} = 1$$

$$\phi_{\beta_D}^{R_0} = \frac{\partial R_0}{\partial \beta_D}\frac{\beta_D}{R_0} = \frac{\beta_D}{(\beta_D+\beta_o)'}$$

$$\phi_{\beta_o}^{R_0} = \frac{\partial R_0}{\partial \beta_o}\frac{\beta_o}{R_0} = \frac{\beta_o}{(\beta_D+\beta_o)},$$

$$\phi_\mu^{R_0} = \frac{\partial R_0}{\partial \mu}\frac{\mu}{R_0} = \frac{-(2\mu+\alpha_D+\alpha_o+\gamma+\sigma)}{(\mu+\alpha_D+\alpha_o+\gamma+\sigma)},$$

$$\phi_{\alpha_D}^{R_0} = \frac{\partial R_0}{\partial \alpha_D}\frac{\partial \sigma_D}{R_0} = -\frac{k}{(\mu+\alpha_D+\alpha_o+\gamma+\sigma)}\frac{\alpha_D}{R_0}$$
$$= \frac{k}{(k-1)'}$$

$$\phi_{\alpha_o}^{R_0} = \frac{\partial R_0}{\partial \alpha_o}\frac{\alpha_o}{R_0} = -\frac{\alpha_0}{(\mu+\alpha_D+\alpha_o+\gamma+\sigma)'}$$

$$\phi_\gamma^{R_0} = \frac{\partial R_0}{\partial y}\frac{\gamma}{R_0} = -\frac{\sigma}{(\mu+\alpha_D+\alpha_o+\gamma+\sigma)'}$$

$$\phi_\sigma^{R_0} = \frac{\partial R_0}{\partial \sigma}\frac{\sigma}{R_0} = -\frac{\sigma}{(\mu+\alpha_D+\alpha_o+\gamma+\sigma)}$$

From Table III, we see that R_0 is most sensitive to the parameters A, β_D, and β_o. From this analysis, we conclude that an increase in the transmission rate increases the spread

TABLE III: ELASTICITY INDICES OF R_0

Parameters	Elastic Index	Value
A	$\phi_{\beta}^{R_0}$	1
β_D	$\phi_{\beta_D}^{R_0}$	0.9
β_o	$\phi_{\beta_o}^{R_0}$	0.09
μ	$\phi_{\mu}^{R_0}$	-1.01
γ	$\phi_{\gamma}^{R_0}$	-0.046
k	$\phi_{k}^{R_0}$	-0.25
α_D	$\phi_{\alpha_D}^{R_0}$	-0.18
α_o	$\phi_{\alpha_o}^{R_0}$	-0.37
σ	$\phi_{\sigma}^{R_0}$	-0.37

of COVID-19, and therefore, to prevent the infection from spreading further, control measures should be deployed that reduce the transmission rate. From Table III, we also see that the parameter β_D is more sensitive towards R_0 compared to β_o.

B. Sensitivity Analysis

To evaluate the influence of model parameters on the infected population I, a sensitivity analysis of the model (1)-(5) is performed using the Partial Rank Correlation Coefficient (PRCC) method with the Latin Hypercube Sampling (LHS) technique, as shown in [42]. The analysis assumes a uniform distribution for all parameters, with the infected population I as the response function. PRCC values for the response function I are presented in Fig. 5. A total of 10000 simulations were conducted to estimate PRCC.

PRCC analysis reveals that the most sensitive parameters influencing the infected population $I(t)$ are the transmission rate of the omicron variant (β_o) and the death rate due to the delta variant (α_D). The positive PRCC for β_o indicates that higher omicron transmission significantly increases infections, while the strong negative PRCC for α_D suggests that a higher death rate from the delta variant sharply reduces the infected population. Other parameters, such as the birth rate (A), natural death rate (μ), and contact tracing rate (k), have minimal impact on infection dynamics. The recovery rate (γ) also moderately reduces infections. These findings underscore the importance of managing transmission rates and variant-specific mortality to control the spread of infection.

This study utilized India's total beginning population, N(0) = 1382339513, derived from the data provided in literature [43]. Based on the information provided in [43], as of August 1, 2020, $I(0) = 1401737$, $R(0) = 1184321$, and $Q(0) = 350435$. Consequently, the initial susceptible people were calculated as follows: $S(0) = N(0) - I(0) - Q(0) - R(0) = 1379403021$. For simulation, the estimated parametric values for the COVID-19 case in India were considered as follows [43].

Fig. 6 illustrates the impact of the parameter k on the infected, quarantined and recovered populations. Likewise, Fig. 7 demonstrates the effect of parameter γ on these same groups. Figs. 6 and 7 depict the effects of k and γ on the populations of I, Q, and R over time t, using the parameter values provided in Table IV.

The graph displayed in Fig. 6a represents the population under quarantine for three distinct values of the parameter

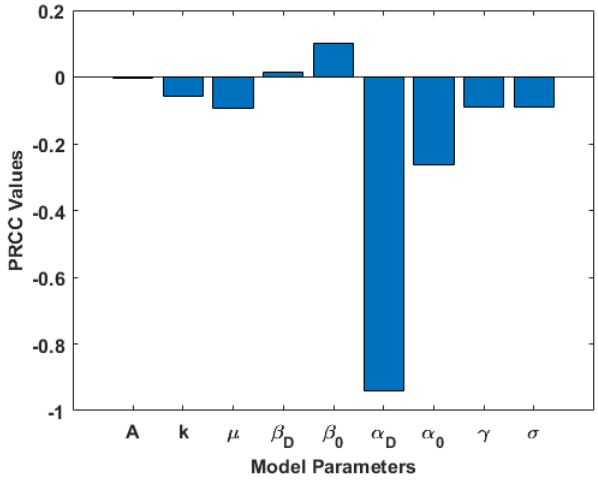

Fig. 5: PRCC sensitivity indices of I against the model parameters for the system (1) -(4)

TABLE IV: LIST OF PARAMETER VALUES-II

Symbols	Values	Source
A	10.48	[43]
k	0.2	assumed
μ	0.00714	[43]
β_D	0.004	[43]
β_o	0.04	Assumed
α_D	0.1	Assumed
α_o	0.022778	[43]
γ	0.3448	[43]
σ	0.475	[43]

k $(0.5, 0.3,$ and $0.1)$ over time (measured in days). The parameter k most often represents the rate of transmission or quarantine effectiveness. The quarantined population peak rises with an increase in the value of k. In particular, the peak is the highest and appears earliest for k = 0.5 (green line), and a sharp decrease follows it. In comparison to k = 0.5, the peak for k = 0.3 (dashed line) is lower and occurs slightly later. The peak is the lowest and appears later, with a more steady decrease, for k = 0.1 (red line). Higher k values generally cause the population under quarantine to peak larger and earlier and to drop more quickly, suggesting a more vigorous outbreak.

A sharp and high peak in the infected population, shown in Fig. 6b, is the outcome of higher values of k, suggesting faster dissemination and higher peak infection rates. A smaller peak is produced by lower values of k, suggesting a slower pace of dissemination and lower peak infection rates. The infected population declines quickly for all values of k despite variations in peak heights, indicating the possibility of successful control strategies or recovery mechanisms. Overall, the graph shows how various transmission rates affect the dynamics of the infected population. Higher transmission rates cause larger and faster peaks in infections, whereas lower transmission rates cause smaller and slightly delayed peaks. As seen from Fig. 6c, the population's rate and degree of recovery are strongly influenced by the parameter k. A faster and more complete recovery is the outcome of higher values of k, whereas a slower and less complete recovery is the result of lower values of k.

The graph in Fig. 7a shows how well recovery and quar-

antine work to stop the disease from spreading. The disease spreads rapidly but is efficiently controlled, as evidenced by the sharp fall in the susceptible population and the matching rise in the quarantine and recovered populations. The fact that there are rarely many sick people at any one time points to the effectiveness of the quarantine regulations in halting the spread of active illnesses. In conclusion, the graph sheds light on the dynamics of the illness and the population's response to confinement and recovery. Faster recovery rates are brought about by higher γ values, which cause the population under quarantine to peak earlier and decline more quickly. A slower recovery rate from lower γ values results in a greater peak in the isolated population that declines more slowly. Over time, the confined population declines for all gamma values; however, the rate of decline accelerates for higher gamma values. The relationship between the dynamics of the quarantined population and the recovery rate (γ) is generally depicted in Fig. 7 demonstrates that higher values of γ result in a faster decline of the infected population. As γ increases, the peak of infection remains nearly the same, but the recovery or removal of infected individuals happens more quickly. This indicates that increasing γ reduces the duration of infection, thereby leading to a more rapid decrease in the infected population over time.

VI. Conclusion

A mathematical model is presented to better understand the newly introduced SARS-CoV-2 virus variant, precisely Delta and the Omicron variants. It is noted that the current model's solution is positive and bounded in time. We then discussed the stability assessment of the equilibrium points admitted by finding the eigenvalues of the Jacobian matrix at each of the equilibrium points. It is observed that for $R_0 < 1$, the model's infection-free equilibrium point is globally asymptotically stable. As R_0 crossed unity, the infection-free equilibrium was found to become unstable. The endemic equilibrium point of the model was found to remain asymptotically stable provided ($M_{11}+M_{22}$) < 0 and $(M_{11}M_{22} - M_{12}M_{21}) > 0$. From the local stability, it is obtained that the virus infection could be managed or controlled by minimizing the value of the R_{D}. To predict the sensitivity of the model parameters on R_0, an elastic index that measures the relative change of R_0 with reference to parameters was calculated for each parameter in the definition of R_0. The susceptible population's birth rate (A) and transmission rates (β_D, β_o) were found to be the most sensitive parameters towards R_0. The theoretical results proved are supported with numerical illustrations in the study.

A sensitivity analysis was conducted to see the influence of parameter value on population dynamics. Overall, it is concluded that faster recovery rates are brought about by higher γ values, which cause the population under quarantine to peak earlier and decline more quickly, whereas the infected population decreases fastly in all situations despite varying γ values, indicating a highly effective reduction in the total number of infected individuals. To evaluate the influence of model parameters on the infected population I, a sensitivity analysis of the model (1) -(4) is performed using the Partial Rank Correlation Coefficient (PRCC) method with the Latin Hypercube Sampling (LHS) technique, as in [42]. The analysis assumes a uniform distribution for all parameters,

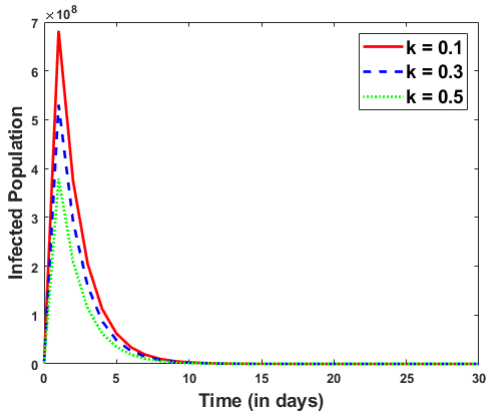

(a) Variation in infected population

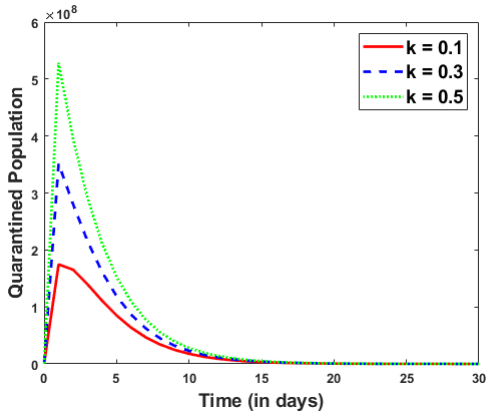

(b) Variation in quarantined population

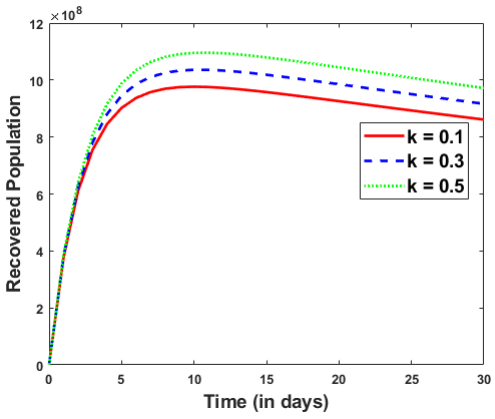

(c) Variation in recovered population

Fig. 6: Variation in population of I, Q and R with respect to time in days for different values of the parameter k

with the infected population I as the response function. The mean strength of the PRCC values, where the sign indicates the correlation between the response function and the model parameters, helps identify significant parameters affecting I. PRCC values for the response function I are presented in Fig. 5. A total of 10000 simulations were conducted to estimate PRCC.

Acknowledgment

The authors would like to thank and acknowledge the support provided by K.R. Mangalam University, Gurugram, India, for offering research facilities for this work.

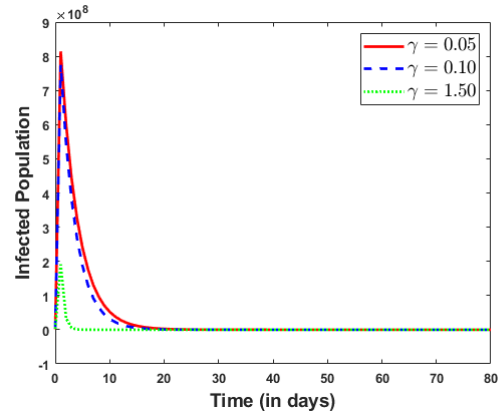

(a) Variation in infected population

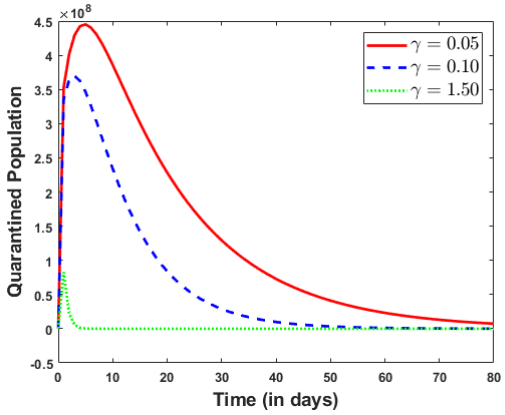

(b) Variation in quarantined population

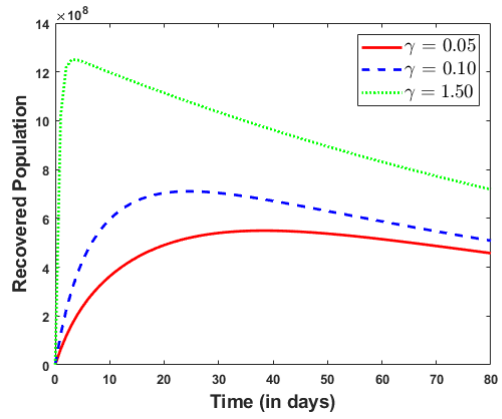

(c) Variation in recovered population

Fig. 7: Variation in population of I, Q and R with respect to time in days for different values of the parameter gamma γ

REFERENCES

[1] D. Chumachenko, I. Meniailov, K. Bazilevych, T. Chumachenko, and S. Yakovlev, "Investigation of statistical machine learning models for COVID-19 epidemic process simulation: Random forest, K-nearest neighbors, gradient boosting," *Computation*, vol. 10, no. 6, p. 86, 2022.

[2] F. Yanuar, M. Q. Shobri, R. F. Mabrur, I. H. Putri, and A. Zetra, "Classification of death risk for COVID-19 patients using bayesian logistic regression and naive bayes classifier," *IAENG International Journal of Computer Science*, vol. 50, no. 3, pp. 915–920, 2023.

[3] A. Quilez-Robres, M. Acero-Ferrero, D. Delgado-Bujedo, R. Lozano-Blasco, and M. Aiger-Valles, "Social networks in military powers: Network and sentiment analysis during the COVID-19 pandemic," *Computation*, vol. 11, no. 6, p. 117, 2023.

[4] I. Cooper, A. Mondal, and C. G. Antonopoulos, "A SIR model assumption for the spread of COVID-19 in different communities," *Chaos, Solitons & Fractals*, vol. 139, p. 110057, 2020.

[5] G. P. Sahu and J. Dhar, "Dynamics of an SEQIHRS epidemic model with media coverage, quarantine and isolation in a community with pre-existing immunity," *Journal of Mathematical Analysis and Applications*, vol. 421, no. 2, pp. 1651–1672, 2015.

[6] W. K. Ming, J. Huang, and C. J. Zhang, "Breaking down of healthcare system: Mathematical modelling for controlling the novel coronavirus (2019-nCoV) outbreak in Wuhan, China," *BioRxiv*, 2020.

[7] S. K. Biswas, J. K. Ghosh, S. Sarkar, and U. Ghosh, "COVID-19 pandemic in India: a mathematical model study," *Nonlinear Dynamics*, vol. 102, pp. 537–553, 2020.

[8] T. M. Chen, J. Rui, Q. P. Wang, Z. Y. Zhao, J. A. Cui, and L. Yin, "A mathematical model for simulating the phase-based transmissibility of a novel coronavirus," *Infectious Diseases of Poverty*, vol. 9, no. 01, pp. 18–25, 2020.

[9] M. Dashtbali and M. Mirzaie, "A compartmental model that predicts the effect of social distancing and vaccination on controlling COVID-19," *Scientific Reports*, vol. 11, no. 1, p. 8191, 2021.

[10] A. Leontitsis, A. Senok, A. Alsheikh Ali, Y. Al Nasser, T. Loney, and A. Alshamsi, "SEAHIR: A specialized compartmental model for COVID-19," *International Journal of Environmental Research and Public Health*, vol. 18, no. 5, p. 2667, 2021.

[11] F. Ndaïrou, I. Area, J. J. Nieto, and D. F. Torres, "Mathematical modeling of COVID-19 transmission dynamics with a case study of Wuhan," *Chaos, Solitons & Fractals*, vol. 135, p. 109846, 2020.

[12] P. Samui, J. Mondal, and S. Khajanchi, "A mathematical model for COVID-19 transmission dynamics with a case study of India," *Chaos, Solitons & Fractals*, vol. 140, p. 110173, 2020.

[13] K. Sarkar, S. Khajanchi, and J. J. Nieto, "Modeling and forecasting the COVID-19 pandemic in India," *Chaos, Solitons & Fractals*, vol. 139, p. 110049, 2020.

[14] A. Zeb, E. Alzahrani, V. S. Erturk, and G. Zaman, "Mathematical model for coronavirus disease 2019 (COVID-19) containing isolation class," *BioMed Research International*, vol. 2020, no. 1, p. 3452402, 2020.

[15] Z. Y. Zhao, Y. Z. Zhu, J. W. Xu, S. X. Hu, Q. Q. Hu, Z. Lei, J. Rui, X. C. Liu, Y. Wang, M. Yang *et al.*, "A five-compartment model of age-specific transmissibility of SARS-CoV-2," *Infectious Diseases of Poverty*, vol. 9, pp. 1–15, 2020.

[16] S. Bahri, A. Mardiyah, A. I. Baqi, and A. Zakiyyah, "Local stability analysis and simulation of omicron virus spread using the omicron SSvIR model," *IAENG International Journal of Applied Mathematics*, vol. 54, no. 5, pp. 797–803, 2024.

[17] J. Suksamran, S. Amornsamankul, and Y. Lenbury, "Reaction-diffusion-integral system modeling SARS-CoV-2 infection-induced versus vaccine-induced immunity: Analytical solutions and stability analysis," *IAENG International Journal of Applied Mathematics*, vol. 54, no. 2, pp. 223–231, 2024.

[18] S. İ. Araz, "Analysis of a COVID-19 model: Optimal control, stability and simulations," *Alexandria Engineering Journal*, vol. 60, no. 1, pp. 647–658, 2021.

[19] M. S. Aronna, R. Guglielmi, and L. M. Moschen, "A model for COVID-19 with isolation, quarantine and testing as control measures," *Epidemics*, vol. 34, p. 100437, 2021.

[20] A. K. Dhaiban and B. K. Jabbar, "An optimal control model of COVID-19 pandemic: a comparative study of five countries," *Opsearch*, vol. 58, no. 4, pp. 790–809, 2021.

[21] R. Djidjou-Demasse, Y. Michalakis, M. Choisy, M. T. Sofonea, and S. Alizon, "Optimal COVID-19 epidemic control until vaccine deployment," *MedRxiv*, pp. 2020–04, 2020.

[22] L. Göllmann, D. Kern, and H. Maurer, "Optimal control problems with delays in state and control variables subject to mixed control–state constraints," *Optimal Control Applications and Methods*, vol. 30, no. 4, pp. 341–365, 2009.

[23] G. B. Libotte, F. S. Lobato, G. M. Platt, and A. J. S. Neto, "Determination of an optimal control strategy for vaccine administration in COVID-19 pandemic treatment," *Computer Methods and Programs in Biomedicine*, vol. 196, p. 105664, 2020.

[24] A. Ndondo, S. Kasereka, S. Bisuta, K. Kyamakya, E. Doungmo, and R. M. Ngoie, "Analysis, modeling and optimal control of covid-19 outbreak with three forms of infection in Democratic Republic of the Congo," *Results in Physics*, vol. 24, p. 104096, 2021.

[25] B. Chhetri, V. M. Bhagat, D. Vamsi, V. Ananth, R. Mandale, S. Muthusamy, C. B. Sanjeevi *et al.*, "Within-host mathematical modeling on crucial inflammatory mediators and drug interventions in COVID-19 identifies combination therapy to be most effective and optimal," *Alexandria Engineering Journal*, vol. 60, no. 2, pp. 2491–2512, 2021.

[26] A. Joshi, H. Kaur, L. Krishna, S. Sharma, G. Sharda, G. Lohra, A. Bhatt, and A. Grover, "Tracking COVID-19 burden in India: A review using SMAART RAPID tracker," *Online Journal of Public Health Informatics*, vol. 13, no. 1, p. e4, 2021.

[27] S. Mandal, N. Arinaminpathy, B. Bhargava, and S. Panda, "Plausibility of a third wave of COVID-19 in India: A mathematical modelling based analysis," *Indian Journal of Medical Research*, vol. 153, no. 5-6, pp. 522–532, 2021.
[28] K. Chatterjee, K. Chatterjee, A. Kumar, and S. Shankar, "Healthcare impact of COVID-19 epidemic in India: A stochastic mathematical model," *Medical Journal Armed Forces India*, vol. 76, no. 2, pp. 147–155, 2020.
[29] K. K. Sukandar, A. L. Louismono, M. Volisa, R. Kusdiantara, M. Fakhruddin, N. Nuraini, and E. Soewono, "A prospective method for generating COVID-19 dynamics," *Computation*, vol. 10, no. 7, p. 107, 2022.
[30] C. Zhang, "Supporting decision-making for covid-19 outbreaks with the modified seir model," *IAENG International Journal of Computer Science*, vol. 48, no. 1, pp. 86–95, 2021.
[31] G. González-Parra and A. J. Arenas, "Mathematical modeling of SARS-CoV-2 Omicron wave under vaccination effects," *Computation*, vol. 11, no. 2, p. 36, 2023.
[32] Mayo Clinic, "COVID-19 variants: What's the concern?" https://www.mayoclinic.org/diseases-conditions/coronavirus/expert-answers/covid-variant/faq-20505779, 2024, accessed: 14-Jun-2024.
[33] M. A. Khan and A. Atangana, "Mathematical modeling and analysis of COVID-19: A study of new variant Omicron," *Physica A: Statistical Mechanics and its Applications*, vol. 599, p. 127452, 2022.
[34] J. Oh, C. Apio, and T. Park, "Mathematical modeling of the impact of Omicron variant on the COVID-19 situation in South Korea," *Genomics & Informatics*, vol. 20, no. 2, p. e22, 2022.
[35] A. S. Ciupeanu, M. Varughese, W. C. Roda, D. Han, Q. Cheng, and M. Y. Li, "Mathematical modeling of the dynamics of COVID-19 variants of concern: Asymptotic and finite-time perspectives," *Infectious Disease Modelling*, vol. 7, no. 4, pp. 581–596, 2022.
[36] O. Diekmann, J. Heesterbeek, and M. G. Roberts, "The construction of next-generation matrices for compartmental epidemic models," *Journal of the Royal Society Interface*, vol. 7, no. 47, pp. 873–885, 2010.
[37] C. C. Chavez, Z. Feng, and W. Huang, "On the computation of r_0 and its role on global stability," *Mathematical Approaches for Emerging and Re-emerging Infection Diseases: An Introduction*, vol. 125, pp. 31–65, 2002.
[38] H. Lu, Y. Ding, S. Gong, and S. Wang, "Mathematical modeling and dynamic analysis of SIQR model with delay for pandemic COVID-19," *Mathematical Biosciences and Engineering*, vol. 18, no. 4, pp. 3197–3214, 2021.
[39] H. W. Berhe, O. D. Makinde, and D. M. Theuri, "Parameter estimation and sensitivity analysis of dysentery diarrhea epidemic model," *Journal of Applied Mathematics*, vol. 2019, no. 1, p. e22, 2019.
[40] P. Van den Driessche, "Reproduction numbers of infectious disease models," *Infectious Disease Modelling*, vol. 2, no. 3, pp. 288–303, 2017.
[41] G. P. Sahu and J. Dhar, "Analysis of an SVEIS epidemic model with partial temporary immunity and saturation incidence rate," *Applied Mathematical Modelling*, vol. 36, no. 3, pp. 908–923, 2012.
[42] S. R. Bandekar and M. Ghosh, "Mathematical modeling of COVID-19 in India and Nepal with optimal control and sensitivity analysis," *The European Physical Journal Plus*, vol. 136, pp. 1–25, 2021.
[43] S. Paul, A. Mahata, S. Mukherjee, and B. Roy, "Dynamics of SIQR epidemic model with fractional order derivative," *Partial Differential Equations in Applied Mathematics*, vol. 5, p. 100216, 2022.